Influence of excess silicon on polytype selection during metal-mediated epitaxy of GaN nanowires

A. Liu[1], Z. Xi[1], M. Li[2], J.C. Yang[2,3,4], L. Qi[1] and R. S. Goldman[1,5*]

[1]*Department of Materials Science and Engineering, University of Michigan, Ann Arbor, MI 48109-2136, USA*

[2]*Center for Functional Nanomaterials, Brookhaven National Laboratory, Upton, NY 11973-5000, USA*

[3]*Department of Chemical and Petroleum Engineering, University of Pittsburgh, Pittsburgh, PA 15261, USA*

[4]*Department of Physics and Astronomy, University of Pittsburgh, Pittsburgh, PA 15261, USA*

[5]*Department of Physics, University of Michigan, Ann Arbor, MI 48109-2136, USA*

*rsgold@umich.edu

5/28/2024

Abstract

We have examined the origins of polytype selection during metal-mediated molecular-beam epitaxy of GaN nanowires (NWs). High-angle annular dark-field scanning transmission electron microscopy reveals [111]-oriented zincblende (ZB) NWs and [0001]-oriented wurtzite (WZ) NWs, with Si_xN_y at the interface between individual NWs and the Si (001) substrate. Quantitative energy dispersive x-ray spectroscopy reveals a notably higher Si concentration of 7.0% ± 2.3% in zincblende (ZB) NWs than 2.3% ± 1.2% in wurtzite (WZ) NWs. Meanwhile, density functional theory (DFT) calculations show that incorporation of 8 atomic % Si on the Ga sublattice inverts the difference in formation energies between WZ and ZB GaN, such that the ZB polytype of GaN is stabilized. This identification of Si and other ZB polytype stabilizers will enable the development of polytype heterostructures in a wide variety of WZ-preferring compounds.

Semiconductor polytype heterostructures, which consist of chemically homogeneous structures formed via an abrupt change in atomic plane stacking sequence, offer opportunities for performance exceeding those of composition-based heterostructures.[1–4] For example, it has been suggested that the formation of zincblende (ZB) segments within wurtzite (WZ) nanowires (NWs) can act as quantum dots (QDs) in NWs, which are promising candidate for single-photon emitters.[5] For ZB-polytype preferring materials, such as III-As and III-Sb, NW polytype transformations have been described by empirical contact angle models, apparently enabling the design and fabrication of polytype superlattices.[1,2,6,7] Meanwhile, conflicting findings on the influence of heterovalent impurities on ZB vs. WZ polytype selection have been reported.[8–10] On the other hand, for GaN, a WZ-polytype preferring material, the empirical contact models (incorrectly) predict ZB polytype selection across contact angles, while the influence of heterovalent impurities on polytype selection remains unknown. To date, both ZB and WZ GaN have been grown on GaAs (001),[11,12] Si (111),[13] and sapphire (0001)[14], with ZB nuclei consisting of 10 to 800 nm pyramid-shapes and WZ GaN nucleating on {111} facets.[11–16] In nanostructured GaN, the selection of the metastable ZB polytype has been attributed to surface energy minimization: the surface energy per unit volume is minimized by adoption of the ZB polytype which has a higher density of low energy {111} surface planes in comparison with the WZ polytype.[17–20]

Recently, we discovered a metal-mediated molecular-beam epitaxy (MBE) process to nucleate ensembles of WZ NWs and "WZ-on-ZB" NWs.[21] Key to this process is a Ga pre-deposition step, in which Ga droplet arrays are formed prior to NW growth. For the WZ-on-ZB NW ensembles, reflection high-energy electron diffraction (RHEED) and x-ray diffraction (XRD) suggest an overall ZB-WZ transformation at thickness ~20 nm. However, the atomic structure of individual NWs and the mechanisms for their polytype transformations remains unknown. Here,

we present evidence that Si acts as a ZB polytype stabilizer during the self-catalyzed growth of GaN NWs. Quantitative energy dispersive x-ray spectroscopy (EDS) reveals a higher Si atomic fraction in ZB NWs in comparison to that of WZ NWs. Interestingly, corresponding density functional theory (DFT) calculations predict that incorporation of 8 atomic % Si on the Ga sublattice inverts the difference in formation energies between WZ and ZB GaN, $\Delta E_{ZB\text{-}WZ}$, such that the ZB polytype of GaN is stabilized. Similar inversions of $\Delta E_{ZB\text{-}WZ}$ are computed for Group IVA elements substituting for Ga and Group VIA elements substituting for N. The identification of Si and other ZB polytype stabilizers will enable the development of polytype heterostructures in a wide variety of WZ-preferring compounds.

GaN NW ensembles were prepared on Si (001) substrates using MBE with a Ga effusion cell and a RF N plasma source, as described elsewhere.[21] The metal-mediated epitaxy involved two steps: Ga pre-deposition (3 minutes), followed by nitridation (~3 hours). For the WZ NW ensembles, low Ga beam equivalent pressure (BEP) of 3.0×10^{-8} was used during both steps. On the other hand, for the WZ-on-ZB NW ensembles, a high Ga BEP (1.5×10^{-7} Torr) was used during the Ga pre-deposition step, while a low Ga BEP (3.0×10^{-8}) was used during the nitridation step. The nitrogen flow rate and plasma power were held at 1 sccm and 400W, respectively, generating a nitrogen flux of 1×10^{-6} Torr, as measured by the partial pressure of 14 amu using a residual gas analyzer.

To prepare individual NWs for atomistic visualization, cross-sectional specimens were fabricated using focused ion beam (FIB) lift-out on a Thermo Fisher Scientific Helios G4 Dual Beam system equipped with a Xe-plasma ion source. During the FIB lift-out process, the NW ensembles were coated with C, thereby providing a definition of the NW perimeters, as will be discussed below. High-angle annular dark-field scanning transmission electron microscopy

(HAADF-STEM), annular dark-field STEM (ADF-STEM), and EDS were preformed using a Thermo Fisher Scientific Talos F200X G2 S/TEM operated at 200 kV with a Super-X EDS detector. The HAADF image in Fig. S1 reveals ensembles of vertically-oriented WZ NWs, with average diameters ~ 40 nm and lengths ~ 150 nm, consistent with SEM images in our earlier report.[21] Since the diameter of the smallest selected-area electron diffraction aperture is ~ 200 nm, which is larger than the NW diameters, we instead used fast Fourier transforms (FFTs) of images to determine the local atomic structures. The DFT calculations were conducted using the Vienna Ab-Initio Simulation Package (VASP),[22,23] with an all-electron projector-augmented wave potentials (PAW) method and the Perdew-Burke-Ernzerhof (PBE) exchange-correlation functional.[24,25] For all DFT calculations the norms of all the forces for supercells were converged to 10^{-3} eV/Å for the ionic relaxation loop, and the total energies were converged to 10^{-8} eV for the electronic self-consistency loop using plane-wave cutoff energy of 600.0 eV and Gaussian smearing of 0.05 eV. A $\mathbf{5 \times 6 \times 2}$ Gamma-centered k-point grid with the k-spacing value of ~0.03 Å^{-1} was employed.

In Fig. 1, we present visualizations of the atomic structure of individual NWs from the WZ NW ensembles. The upper panel in Fig. 1 displays the HAADF intensity profile extracted from the red dashed line across the vertically-oriented WZ NW in Fig. 1(a). The local minima, indicated by downward pointing arrows, correspond to the exterior of the NW, thereby providing a definition of the NW perimeter, the white dotted line in Fig. 1(a). Figs. 1(b) and 1(c) are high-resolution views from the regions denoted by white boxes in Fig. 1(a), including (b) a region ~50 nm from the Si-GaN interface and (c) a region that includes the Si-GaN interface. In the insets to Figs. 1(b) and 1(c), blue and pink dots illustrate the ABAB stacking along the [0001] direction, indicative of the WZ polytype. Since the closest-packed (0001) planes are oriented along the Si [001] surface normal and parallel to the growth direction, the WZ GaN NW is [0001]-oriented. Although an

interfacial layer is apparent at the Si-GaN interface (Fig. 1(c)), FFTs of HAADF images (Fig. 1(d)) collected in the vicinity NW/Si interface (such as the location indicated by the green dotted box in Fig. 1(a)) reveal overlapping WZ $[\mathbf{11\bar{2}0}]$ and Si $[\mathbf{110}]$ zone axes, with the WZ [0001] parallel to the Si [001], confirming NW/Si epitaxy. Figs. 1(e) and 1(f) are the FFTs obtained from the pink and purple dashed boxes in Figs. 1(b) and 1(c), respectively; both are indexed to the WZ $[\mathbf{1\bar{1}00}]$.

Visualization of the atomic structures of individual NWs from WZ-on-ZB NW ensembles are shown in Fig. 2. The upper panel in Fig. 2 displays the HAADF intensity profile extracted from the red dashed line in Fig. 2(a). Similar to the case for Fig. 1, the local minima, indicated by downward pointing arrows, correspond to the NW exterior, thereby defining the NW perimeter, the white dotted line in Fig. 2(a). Interestingly, the WZ-on-ZB NW is oriented at 53° with respect to the Si (001) direction. Figs. 2(b) and 2(c) are high-resolution views from the regions denoted by white boxes in Fig. 2(a), including (b) a region ~20 nm from the Si-GaN interface and (c) a region at the Si-GaN interface. In the inset to Fig. 2(c), blue, pink, and yellow dots illustrate the ABC stacking along the [111] direction, suggesting the presence of the ZB polytype. The FFT taken from the green dashed box in Fig. 2(c), shown in Fig. 2(d), reveals overlapping ZB $[\mathbf{\bar{1}10}]$and Si [110] zone axes, with the ZB [111] parallel to the Si [001], confirming NW/Si epitaxy. Figs. 2(e) and 2(f) are FFTs obtained from the pink and purple dashed boxes in Fig. 2(b). Since the purple box is indexed to ZB $[\mathbf{\bar{1}10}]$ (Fig. 2(f)) and the pink box is indexed to WZ $[\mathbf{11\bar{2}0}]$ (Fig. 2(e)), a ZB-to-WZ polytype transformation has occurred in Fig. 2(b), with both ZB [111] and WZ [0001] parallel to the NW growth direction. Since the NW growth axis is approximately 53° from the Si [001] surface normal, the ZB (001) planes are parallel to Si (001) surface normal. To complement this analysis, high-resolution STEM images of an additional WZ-on-ZB NW are provided in Fig. S2. As will be discussed below, [0001]-oriented WZ NWs are occasionally

observed in the WZ-on-ZB NW ensembles, presumably due to local variations in surface Ga concentration during the growth.

We now examine the elemental distribution in WZ and ZB NWs using two-dimensional EDS mapping. Figs. 3(a) and 3(b) present HAADF images and EDS maps collected in the vicinity of the NW/Si interfaces, with grey dotted lines outlining "lattice-fringe-free" layers at the interface between the Si substrate and the WZ and ZB NWs, respectively. In both Figs. 3(a) and 3(b), the EDS maps reveal that the purple (Ga) pixels are primarily confined to the NW regions. However, the blue (Si) pixels are apparent in both the substrate and interface layers, while the pink (N) pixels are located in both the interface layers and the NW regions, suggesting the presence of Si_xN_y at the Si/NW interface. Although this interfacial Si_xN_y layer was not evident in our earlier studies which emphasized the average structure,[21] it is likely due to post-epitaxy diffusion of N from GaN to the Si substrate.[26] Furthermore, the presence (absence) of Si_xN_y interlayers associated with formation of WZ (ZB) GaN NWs has also been reported.[16] In our case, Si_xN_y interlayers with similar thicknesses are present in the vicinity of both WZ and ZB NWs, suggesting that they have not directly influenced polytype selection.

Although the NW regions appear to consist primarily of nearly 1:1 Ga:N, semi-quantitative EDS reveals the presence of Si within the NW regions. Since the NWs were grown without a Si flux, it is likely that Si diffused from the substrate during growth. Using ~100 nm^2 sized regions in the vicinity of multiple NW/substrate interfaces, such as the yellow boxes in Figs. 3(a) and 3(b), we quantified the Si atomic fraction in individual WZ and ZB NWs. The resulting atomic fractions are shown in the right panels in Figs. 3(a) and 3(b). Interestingly, for the WZ NW, shown in Fig. 3(a), the Si atomic fraction is 0.028 ± 0.001, whereas in the ZB NW, shown in Fig. 3(b), the Si atomic fraction is notably higher, 0.073 ± 0.1. A similar approach was used for multiple WZ and

ZB NWs, with total WZ and ZB NW "footprints" exceeding 4000 nm^2. Notably, the average Si atomic fraction in WZ NWs is 0.023 ± 0.012, whereas ZB NWs show a higher average Si atomic fraction of 0.07 ± 0.023. To minimize artifacts in semi-quantitative EDS analysis, we also compared ZB and WZ NWs from the "WZ-on-ZB NW" ensembles mentioned above. For the WZ NWs, the Si atomic fraction is 0.034 ± 0.005, nearly half the value of the Si atomic fraction in the ZB NWs (0.070 ± 0.023). A complete summary of the Si atomic fractions for individual WZ and ZB NWs is provided in Table S1. We note that absolute Si atomic fractions are difficult to quantify due to multi-scattering and/or delocalization of x-ray signals during EDS in STEM; however, these data offer valuable insights into the trends in Si atomic fractions within the two NW polytypes. We hypothesize that Si influences polytype selection during NW nucleation. Although a Si flux was not provided during the NW growth, Si atoms from the substrate likely dissolved into liquid Ga during the Ga pre-deposition step, with these excess Si atoms leading to the preferential nucleation of ZB GaN NWs.

To consider the predicted impact of Si atoms on selective nucleation of ZB GaN NWs, we employed zero-K DFT calculations within orthorhombic supercells, each comprising 48 atoms. The supercells are illustrated in Figs. 4(a) (WZ oriented along the directions of x $[11\bar{2}0]$, y $[1\bar{1}00]$, and z $[0001]$) and 4(b) (ZB oriented along the directions of x $[\bar{1}10]$, y $[\bar{1}\bar{1}2]$, and z $[111]$). For these calculations, zero, one, or two Si atoms are incorporated into the supercells by random substitutions of Ga atoms. In the absence of Si (pure GaN), the difference in formation energies between ZB and WZ polytypes, $\Delta E_{ZB\text{-}WZ}$, is 5.08 $\times 10^{-3}$ eV/atom, consistent with the reported thermodynamic stability of WZ GaN.[27,28] The introduction of one and two Si atoms, corresponding to Si atomic fractions of 0.042 and 0.083, shrinks $E_{ZB\text{-}WZ}$ to 1.76 $\times 10^{-3}$ eV/atom and -2.95$\times 10^{-3}$ eV/atom, respectively. For the case of two Si atoms, the negative value of $\Delta E_{ZB\text{-}WZ}$ suggests that

the ZB polytype of GaN is stabilized. Due to the high melting temperature of GaN (2,500 °C), the effects of Si on polytype stabilization revealed by these zero-K DFT calculations are expected be applicable to our ~800 °C growth temperature.

We now discuss the impact of the variations in Si atomic fractions on the WZ and WZ-on-ZB NWs ensembles. During metal-mediated epitaxy at ~800 °C, a Si atomic fraction of 0.05 is predicted to be soluble in the Ga-Si liquid phase.[29] For the WZ NW ensembles, the low Ga BEP during the Ga pre-deposition step likely leads to fewer Si atoms dissolved into liquid Ga, resulting in the formation of the WZ polytype. On the other hand, for the WZ-on-ZB NW ensembles, the high Ga BEP during the Ga pre-deposition step enables the dissolving of excess Si into the liquid Ga, resulting in the formation of the ZB polytype. However, once the Si in liquid Ga is consumed, transformation to the WZ polytype is observed, as illustrated in Fig. 2(d).

Beyond examining the influence of Si on WZ vs. ZB polytype stability in GaN, we performed a DFT screening to evaluate the influence of main group elements from the first five periods and transition elements in the fourth period of the periodic table, introduced either as Ga or N substitutions. For Ga substitutions, we considered Mg, Al, Ca, Sc, Ti, V, Cr, Mn, Fe, Co, Ni, Cu, Zn, Ge, In, and Sn. For N substitutions, the elements included were C, O, P, S, As, Se, and Te (See Table S2 in Supplementary Material). As shown in Fig. 4(c), our search predicts that Group IVA elements (blue) substituting for Ga serve as ZB-stabilizers, while Group VIA elements (orange) substituting for N act as ZB-stabilizers.

In summary, we have examined the origins of polytype selection during metal-mediated epitaxy of GaN NWs. High-angle annular dark-field imaging reveals [111]-oriented ZB NWs and [0001]-oriented WZ NWs, with Si_xN_y at the interface between individual NWs and the Si (001) substrate. Quantitative EDS reveals a notably higher average Si atomic fraction in ZB NWs than

in WZ NWs. Correspondingly, DFT calculations predict that incorporation of Si atomic fractions > 0.08 onto the Ga sublattice stabilizes ZB GaN. We hypothesize that the high Ga BEP during the Ga pre-deposition enables dissolution of excess Si into the liquid Ga, thereby stabilizing ZB GaN. Furthermore, our calculations predict that Group IVA elements substituting for Ga and Group VIA elements substituting for N act as ZB stabilizers. The identification of ZB polytype stabilizers will enable the development of polytype heterostructures in a wide variety of WZ-preferring compounds.

Supplementary Material

See the supplementary material for STEM data, including a low-magnification HAADF-STEM image of WZ NW ensembles, HAADF-STEM images of an additional WZ-on-ZB NW, and EDS-determined Si atomic fractions (with error bars) for individual WZ and ZB NWs. In addition, a summary of the DFT-computed $\Delta E_{ZB\text{-}WZ}$ for GaN containing Group IVA (VIA) elements substituting for Ga (N) is presented.

Acknowledgement

This work was supported by the Department of Energy, Basic Energy Sciences under Award # DE-SC0023222. The authors acknowledge the assistance of the staff at the Michigan Center for Materials Characterization at the University of Michigan. This research used Electron Microscopy resources of the Center for Functional Nanomaterials (CFN), which is a U.S. Department of Energy Office of Science User Facility, at Brookhaven National Laboratory under Contract No. DE-SC0012704. Scientific discussions with D. Zakharov are gratefully acknowledged.

References

[1] G. Jacopin, L. Rigutti, L. Largeau, F. Fortuna, F. Furtmayr, F.H. Julien, M. Eickhoff, and M. Tchernycheva, "Optical properties of wurtzite/zinc-blende heterostructures in GaN nanowires," J. Appl. Phys. 110, 064313 (2011).

[2] K. Pemasiri, M. Montazeri, R. Gass, L.M. Smith, H.E. Jackson, J. Yarrison-Rice, S. Paiman, Q. Gao, H.H. Tan, C. Jagadish, X. Zhang, and J. Zou, "Carrier Dynamics and Quantum Confinement in type II ZB-WZ InP Nanowire Homostructures," Nano Lett. 9, 648 (2009).

[3] I. Geijselaers, N. Vainorius, S. Lehmann, C.E. Pryor, K.A. Dick, and M.-E. Pistol, "Atomically sharp, crystal phase defined GaAs quantum dots," Appl. Phys. Lett. 119, 263102 (2021).

[4] A. Jash, S. Lehmann, K.A. Dick, A. Gustafsson, and M.-E. Pistol, "Excitonic Dynamics at the Type-II Polytype Interface of InP Platelets," ACS Photonics 10, 3143 (2023).

[5] B. Loitsch, J. Winnerl, G. Grimaldi, J. Wierzbowski, D. Rudolph, S. Morkötter, M. Döblinger, G. Abstreiter, G. Koblmüller, and J.J. Finley, "Crystal Phase Quantum Dots in the Ultrathin Core of GaAs–AlGaAs Core–Shell Nanowires," Nano Lett. 15, 7544 (2015).

[6] D. Jacobsson, F. Panciera, J. Tersoff, M.C. Reuter, S. Lehmann, S. Hofmann, K.A. Dick, and F.M. Ross, "Interface dynamics and crystal phase switching in GaAs nanowires," Nature 531, 317 (2016).

[7] F. Panciera, Z. Baraissov, G. Patriarche, V.G. Dubrovskii, F. Glas, L. Travers, U. Mirsaidov, and J.-C. Harmand, "Phase Selection in Self-catalyzed GaAs Nanowires," Nano Lett. 20, 1669 (2020).

[8] Y. Zhang, Z. Sun, A.M. Sanchez, M. Ramsteiner, M. Aagesen, J. Wu, D. Kim, P. Jurczak, S. Huo, L.J. Lauhon, and H. Liu, "Doping of Self-Catalyzed Nanowires under the Influence of Droplets," Nano Lett. 18, 81 (2018).

[9] R.E. Algra, M.A. Verheijen, M.T. Borgström, L.-F. Feiner, G. Immink, W.J.P. Van Enckevort, E. Vlieg, and E.P.A.M. Bakkers, "Twinning superlattices in indium phosphide nanowires," Nature 456, 369 (2008).

[10] E. Diak, A. Thomas, V.G. Dubrovskii, and R.R. LaPierre, "Ultrathin Te-Doped GaP Nanoantenna with Crystal Phase Transitions," Cryst. Growth Des. 23, 5074 (2023).

[11] S. Suandon, S. Sanorpim, K. Yoodee, and K. Onabe, "Effect of growth temperature on polytype transition of GaN from zincblende to wurtzite," Thin Solid Films 515, 4393 (2007).

[12] F. Ruiz-Zepeda, Y.L. Casallas-Moreno, J. Cantu-Valle, D. Alducin, U. Santiago, M. José-Yacaman, M. López-López, and A. Ponce, "Precession electron diffraction-assisted crystal phase mapping of metastable c-GaN films grown on (001) GaAs," Microsc. Res. Tech. 77, 980 (2014).

[13] V.V. Fedorov, A.D. Bolshakov, D.A. Kirilenko, A.M. Mozharov, A.A. Sitnikova, G.A. Sapunov, L.N. Dvoretckaia, I.V. Shtrom, G.E. Cirlin, and I.S. Mukhin, "Droplet epitaxy mediated growth of GaN nanostructures on Si (111) *via* plasma-assisted molecular beam epitaxy," CrystEngComm 20, 3370 (2018).

[14] S. Lee, Y. Sohn, C. Kim, D.R. Lee, and H.-H. Lee, "Nanostructural analysis of GaN tripods and hexapods grown on *c* -plane sapphire," J. Appl. Crystallogr. 43, 1300 (2010).

[15] J. Borysiuk, Z.R. Zytkiewicz, M. Sobanska, A. Wierzbicka, K. Klosek, K.P. Korona, P.S. Perkowska, and A. Reszka, "Growth by molecular beam epitaxy and properties of inclined GaN nanowires on Si(001) substrate," Nanotechnology 25 135610 (2014).

[16] A. Wierzbicka, G. Tchutchulashvili, M. Sobanska, K. Klosek, R. Minikayev, J.Z. Domagala, J. Borysiuk, and Z.R. Zytkiewicz, "Arrangement of GaN nanowires on Si(001)

substrates studied by X-ray diffraction: Importance of silicon nitride interlayer," Appl. Surf. Sci. 425, 1014 (2017).

[17] A.W. Wood, R.R. Collino, B.L. Cardozo, F. Naab, Y.Q. Wang, and R.S. Goldman, "Formation mechanisms of spatially-directed zincblende gallium nitride nanocrystals," J. Appl. Phys. 110, 124307 (2011).

[18] S.B. Lee, S.J. Yoo, K. Kim, Y.-S. Kim, Y.-M. Kim, J.-G. Kim, and H.N. Han, "Stabilization of a Ga-adlayer structure with the zincblende stacking sequence in the GaN(0 0 0 −1) surface at the nanoscale," Nanoscale 9, 2596 (2017).

[19] R. Armitage, K. Nishizono, J. Suda, and T. Kimoto, "Mechanism of stabilization of zincblende GaN on hexagonal substrates: Insight gained from growth on ZrB2 (0 0 0 1)," J. Cryst. Growth 284, 369 (2005).

[20] X. Weng, S.J. Clarke, W. Ye, S. Kumar, R.S. Goldman, A. Daniel, R. Clarke, J. Holt, J. Sipowska, A. Francis, and V. Rotberg, "Evolution of structural and optical properties of ion-beam synthesized GaAsN nanostructures," J. Appl. Phys. 92, 4012 (2002).

[21] H. Lu, S. Moniri, C. Reese, S. Jeon, A. Katcher, T. Hill, H. Deng, and R.S. Goldman, "Influence of gallium surface saturation on GaN nanowire polytype selection during molecular-beam epitaxy," Appl. Phys. Lett. 119, 031601 (2021).

[22] G. Kresse, and J. Furthmüller, "Efficiency of ab-initio total energy calculations for metals and semiconductors using a plane-wave basis set," Comput. Mater. Sci. 6, 15 (1996).

[23] G. Kresse, and J. Furthmüller, "Efficient iterative schemes for *ab initio* total-energy calculations using a plane-wave basis set," Phys. Rev. B 54, 11169 (1996).

[24] P.E. Blöchl, "Projector augmented-wave method," Phys. Rev. B 50, 17953 (1994).

[25] J.P. Perdew, K. Burke, and M. Ernzerhof, "Generalized Gradient Approximation Made Simple," Phys. Rev. Lett. 77, 3865 (1996).

[26] L. Cerutti, J. Ristić, S. Fernández-Garrido, E. Calleja, A. Trampert, K.H. Ploog, S. Lazic, and J.M. Calleja, "Wurtzite GaN nanocolumns grown on Si(001) by molecular beam epitaxy," Appl. Phys. Lett. 88, 213114 (2006).

[27] C.-Y. Yeh, Z.W. Lu, S. Froyen, and A. Zunger, "Zinc-blende–wurtzite polytypism in semiconductors," Phys. Rev. B 46, 10086 (1992).

[28] T. Ito, "Simple Criterion for Wurtzite-Zinc-Blende Polytypism in Semiconductors," Jpn. J. Appl. Phys. 37, L1217 (1998).

[29] R.W. Olesinski, N. Kanani, and G.J. Abbaschian, "The Ga−Si (Gallium-Silicon) system," Bull. Alloy Phase Diagr. 6, 362 (1985).

Figures

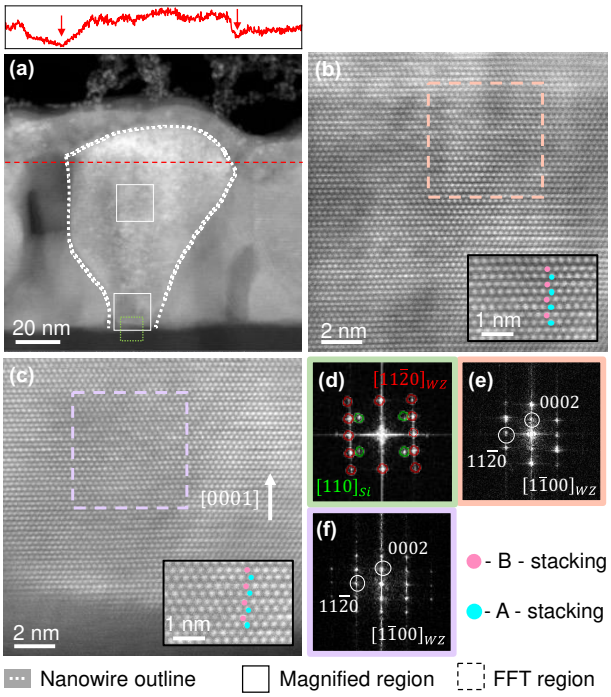

Fig. 1 Individual WZ NW from WZ NW ensembles: (a) High-angle annular-dark-field scanning transmission electron microscopy (HAADF-STEM) image of a WZ NW. The upper panel displays the HAADF intensity profile extracted from the red dashed line in (a). The local minima, indicated by downward pointing arrows, correspond to the NW exterior, thereby defining the NW perimeter, the white dotted line in (a). Atomic-resolution HAADF-STEM images obtained at the white boxes: (b) ~50nm from and (c) near the Si-GaN interface. The insets in (b) and (c) provide close-up views, with blue/pink dots illustrating ABAB stacking. (d) Fast-Fourier Transforms (FFTs) from HAADF images at the NW/Si interface (such as green dotted box in (a)) reveal overlapping WZ $[11\bar{2}0]$

and Si [**110**] zone axes, with WZ [0001] parallel to Si [001], confirming NW/Si epitaxy. FFTs from the (b) pink and (c) purple dashed boxes, shown in (e) and (f) are both indexed to WZ[$\mathbf{1\bar{1}00}$].

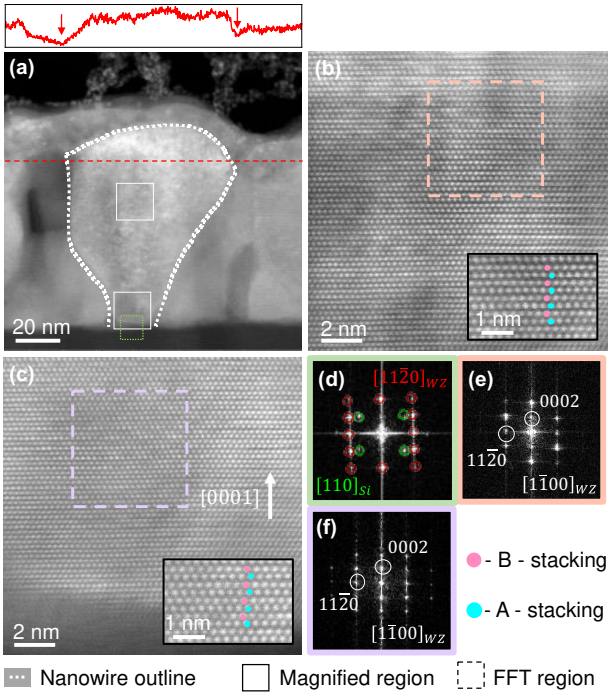

Fig. 2 Individual WZ-on-ZB NW from WZ-on-ZB NW ensembles: (a) High-angle annular-dark-field scanning transmission electron microscopy (HAADF-STEM) image of WZ-on-ZB NW. The upper panel displays the HAADF intensity profile extracted from the red dashed line in (a). The local minima, indicated by downward pointing arrows, correspond to the NW exterior, thereby defining the NW perimeter, the white dotted line in (a). Atomic-resolution images obtained at white boxes: (b) ~20 nm from and (c) at the Si-GaN interface. The inset in (c) provides a close-up view, with blue, pink, and yellow dots illustrating ABC stacking. (d) Fast-Fourier Transform (FFT)

from the green dashed box (NW/Si interface) reveals overlapping ZB$[\bar{1}10]$ and Si [110] zone axes, with ZB[001] parallel to Si[001], confirming NW/Si epitaxy. FFTs from the pink and purple dashed boxes in (b) are indexed to (e) WZ$[11\bar{2}0]$ and (f) ZB$[\bar{1}10]$, revealing the ZB-to-WZ polytype transformation.

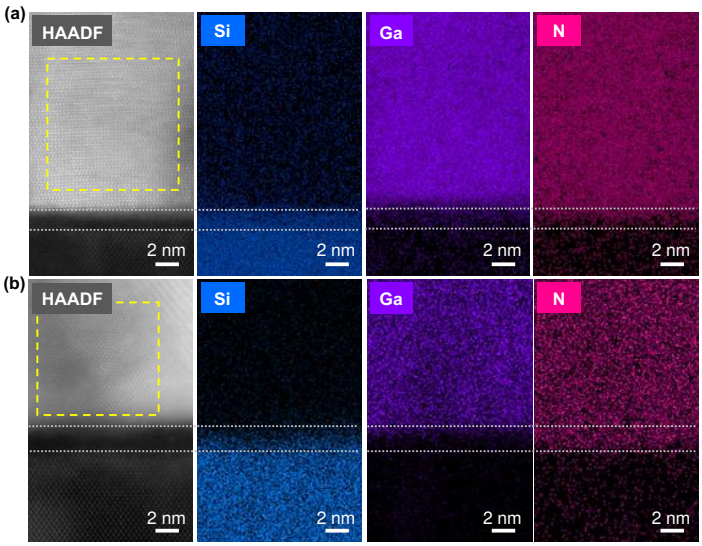

	Atomic Fraction
Si	0.028 ± 0.001
Ga	0.481 ± 0.03
N	0.491 ± 0.03

	Atomic Fraction
Si	0.073 ± 0.01
Ga	0.465 ± 0.03
N	0.462 ± 0.03

Fig 3 High-angle annular-dark-field scanning transmission electron microscopy (HAADF-STEM) images and corresponding energy-dispersive spectroscopy (EDS) data from the (a) WZ and (b) ZB NW, with elemental maps of Si (blue), Ga (purple), and N (pink). The Si_xN_y interfacial layers are outlined by grey dotted lines in (a) and (b). Quantification of EDS data is extracted from the yellow dashed boxes in (a) and (b), as shown in the right panels.

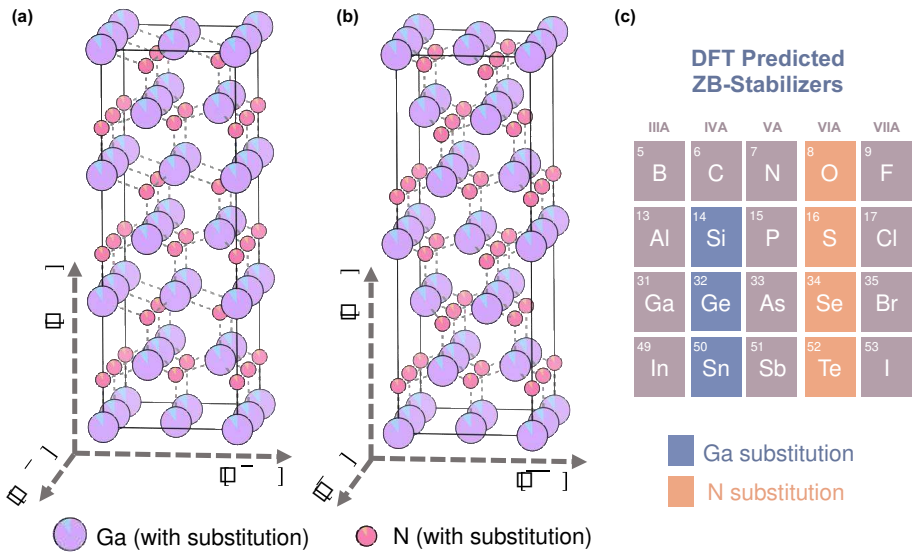

Fig. 4. Illustrations of WZ and ZB GaN supercells and elements of DFT-suggested ZB-stabilizers. (a) and (b) are schematic diagrams of model GaN supercells applied for the energy calculations. Purple-blue-filled circles indicate Ga atoms and their substitutions, while pink-orange-filled circles denote N atoms and their substitutions. The WZ supercell (a) aligns with $\mathbf{x}\,[11\bar{2}0]$, $\mathbf{y}\,[1\bar{1}00]$, and $\mathbf{z}\,[0001]$ directions, whereas the ZB supercell (b) aligns with $\mathbf{x}\,[\bar{1}10]$, $\mathbf{y}\,[\bar{1}\bar{1}2]$, and $\mathbf{z}\,[111]$ directions. (c) Elements from periods 2-4 and groups IIIA-VIIA of the periodic table. ZB-stabilizers of Ga substitution are marked by blue, while N substitution stabilizers are highlighted in orange.